*Clinical Infectious Diseases*

MAJOR ARTICLE

# Coinfection by Severe Acute Respiratory Syndrome Coronavirus 2 and Influenza A(H1N1)pdm09 Virus Enhances the Severity of Pneumonia in Golden Syrian Hamsters

**Anna Jinxia Zhang,[1,a] Andrew Chak-Yiu Lee,[1,a] Jasper Fuk-Woo Chan,[1,2,3,a] Feifei Liu,[1] Can Li,[1] Yanxia Chen,[1] Hin Chu,[1] Siu-Ying Lau,[1] Pui Wang,[1] Chris Chung-Sing Chan,[1] Vincent Kwok-Man Poon,[1] Shuofeng Yuan,[1] Kelvin Kai-Wang To,[1,2,3] Honglin Chen,[1] and Kwok-Yung Yuen[1,2,3]**

[1]State Key Laboratory of Emerging Infectious Diseases, Carol Yu Centre for Infection, Department of Microbiology, Li Ka Shing Faculty of Medicine, The University of Hong Kong, Pokfulam, Hong Kong Special Administrative Region, China, [2]Department of Clinical Microbiology and Infection Control, University of Hong Kong–Shenzhen Hospital, Shenzhen, China, and [3]Department of Microbiology, Queen Mary Hospital, Pokfulam, Hong Kong Special Administrative Region, China

**(See the Editorial Commentary by Covin and Rutherford on pages e993–4.)**

***Background.*** Clinical outcomes of the interaction between the co-circulating pandemic severe acute respiratory syndrome coronavirus 2 (SARS-CoV-2) and seasonal influenza viruses are unknown.

***Methods.*** We established a golden Syrian hamster model coinfected by SARS-CoV-2 and mouse-adapted A(H1N1)pdm09 simultaneously or sequentially. The weight loss, clinical scores, histopathological changes, viral load and titer, and serum neutralizing antibody titer were compared with hamsters challenged by either virus.

***Results.*** Coinfected hamsters had more weight loss, more severe lung inflammatory damage, and tissue cytokine/chemokine expression. Lung viral load, infectious virus titers, and virus antigen expression suggested that hamsters were generally more susceptible to SARS-CoV-2 than to A(H1N1)pdm09. Sequential coinfection with A(H1N1)pdm09 one day prior to SARS-CoV-2 exposure resulted in a lower lung SARS-CoV-2 titer and viral load than with SARS-CoV-2 monoinfection, but a higher lung A(H1N1)pdm09 viral load. Coinfection also increased intestinal inflammation with more SARS-CoV-2 nucleoprotein expression in enterocytes. Simultaneous coinfection was associated with delay in resolution of lung damage, lower serum SARS-CoV-2 neutralizing antibody, and longer SARS-CoV-2 shedding in oral swabs compared to that of SARS-CoV-2 monoinfection.

***Conclusions.*** Simultaneous or sequential coinfection by SARS-CoV-2 and A(H1N1)pdm09 caused more severe disease than monoinfection by either virus in hamsters. Prior A(H1N1)pdm09 infection lowered SARS-CoV-2 pulmonary viral loads but enhanced lung damage. Whole-population influenza vaccination for prevention of coinfection, and multiplex molecular diagnostics for both viruses to achieve early initiation of antiviral treatment for improvement of clinical outcome should be considered.

**Keywords.** coronavirus; COVID-19; SARS-CoV-2; monoinfection; coinfection; influenza; hamster.

The pandemic of coronavirus disease 2019 (COVID-19), caused by severe acute respiratory syndrome coronavirus 2 (SARS-CoV-2), has affected >50 million people with >1.2 million deaths in the last 10 months [1]. SARS-CoV-2 emerged in December 2019 as a cluster of cases of pneumonia related to a food market in the city of Wuhan, China. High person-to-person transmissibility has been demonstrated in intrafamilial settings [2] and other indoor settings with suboptimal ventilation where people gather together without mask protection such as in eateries, bars, cruise ships, fitness clubs, conference halls, workplace pantries, religious premises, and elderly homes [3–5]. Though >60% of COVID-19 patients develop symptoms at some point in time, 4.2%–44% of transmissions can occur during the presymptomatic stage of infection [6]. Moreover, the SARS-CoV-2 viral load often peaks around symptom onset or at presentation of COVID-19 instead of around day 10 after symptom onset as in the case of 2003 SARS, which hampers the efficacy of isolation and contact tracing [7, 8]. Clinical manifestations of COVID-19 vary from mild upper respiratory symptoms to progressive lower respiratory involvement, which can terminate in respiratory failure and multiorgan involvement. The COVID-19 syndrome is not clinically or pathologically distinct from influenza. While seasonal influenza has a crude case fatality rate of 0.1%–0.2%, the estimated crude mortality rate of COVID-19 is around 1%–2% [9, 10]. Both cause severe disease in elderly,

Received 8 November 2020; editorial decision 12 November 2020; published online 20 November 2020.

[a]A. J. Z., A. C.-Y. L., and J. F.-W. C. contributed equally to this work.

Correspondence: K.-Y. Yuen, State Key Laboratory of Emerging Infectious Diseases, Carol Yu Centre for Infection, Department of Microbiology, Li Ka Shing Faculty of Medicine, University of Hong Kong, Pokfulam, Hong Kong SAR, China (kyyuen@hku.hk).

**Clinical Infectious Diseases® 2021;72(12):e978–92**



DOI: 10.1093/cid/ciaa1747

comorbid, and obese patients [11]. As the winter influenza season of 2020 is approaching, we are anticipating an increasing number of coinfections with COVID-19. In a meta-analysis, 3% of hospitalized COVID-19 patients had coinfections with other respiratory viruses of which respiratory syncytial virus and influenza A virus were the most common [12]. Analysis of cases of influenza and COVID-19 coinfections in United Kingdom national surveillance showed that coinfected patients had a 5.9 times greater risk of death [13]. Moreover, mathematical modeling suggested that the decrease of COVID-19 cases in the spring of 2020 was not only related to epidemiological control measures but also to the end of the influenza season, and that influenza may have increased transmission of SARS-CoV-2 by 2- to 2.5-fold [14]. Furthermore, coinfection of guinea pigs by the 2003 SARS coronavirus and a human reovirus isolated from a SARS patient has resulted in more rapid animal death from diffuse alveolar damage [15]. Previously, we set up the golden Syrian hamster model of COVID-19 by intranasal inoculation with SARS-CoV-2, which reproduces the clinical signs, pathological changes, serological response, and transmissibility of this viral pneumonia [16, 17]. Coincidentally, hamsters were found susceptible to infection by the 2009 pandemic H1N1 virus [A(H1N1)pdm09] and other seasonal influenza viruses with weight loss, infectious viral shedding, and viral antigen expression in the respiratory tract [18]. In this study, we titrated for the lower dose of virus inoculum of A(H1N1)pdm09 or SARS-CoV-2 that can cause significant histopathological changes of viral pneumonia in hamsters. The clinical scores, weight loss, histopathological changes, immunohistochemical antigen expression pattern, degree of individual virus replication, and serological responses in hamsters coinfected by both viruses either simultaneously or sequentially are described and analyzed.

## MATERIALS AND METHODS

### Viruses, Cell Lines, and Biosafety

The SARS-CoV-2 HKU-13 strain (GenBank accession number MT835140) was isolated from a COVID-19 patient [19]. The influenza virus was a mouse-adapted strain of A(H1N1)pdm09 named A/HK/415742/2009 [20]. Virus stocks were prepared and titrated for plaque-forming units (PFUs) in Vero E6 cells for SARS-CoV-2 or Madin-Darby canine kidney (MDCK) cells for A(H1N1)pdm09. All experiments involving live SARS-CoV-2 were performed in a Biosafety Level 3 facility at the University of Hong Kong (HKU) following approved standard operating procedures.

### Animals

Male and female Syrian hamsters, aged 6–8 weeks, were obtained from the Chinese University of Hong Kong Laboratory Animal Service Centre through the HKU Centre for Comparative Medicine Research. All the animal experimental procedures were approved by the Committee on the Use of Live Animals in Teaching and Research of HKU.

### Intranasal Inoculation of Hamsters With SARS-CoV-2 and/or A(H1N1) pdm09

The virus stock was diluted in phosphate-buffered saline (PBS) to a total volume of 50 µL inoculum and intranasally inoculated into hamsters under ketamine (200 mg/kg) and xylazine (10 mg/kg) anesthesia [16]. Mock-infected animals were given the same volume of PBS. For monoinfection experiments, inocula of $10^2$, $10^4$, or $10^6$ PFUs of A(H1N1)pdm09, or 10 or $10^3$ PFUs of SARS-CoV-2, were used. In the coinfection study, $10^3$ PFUs of SARS-CoV-2 and $10^5$ PFUs of A(H1N1)pdm09 were used for the high inoculum group; 10 PFUs of SARS-CoV-2 and $10^4$ PFUs of A(H1N1)pdm09 were used for the low inoculum group. For simultaneous coinfection, the 2 viruses were mixed together into 50 µL of inoculum for each animal. For sequential low inoculum coinfection, the second virus inoculum was given 24 hours after the first virus challenge (Figure 1A). Animals were monitored for clinical signs and body weight. At 4, 7, and 14 days postinfection (dpi), 3 animals in each group were euthanized by intraperitoneal injection of pentobarbital sodium (200 mg/kg). Blood and organ tissues were sampled for virological and histopathological analyses.

### Determination of Viral Load by Real-Time Reverse-Transcription Polymerase Chain Reaction and Plaque Assay

Lung and nasal turbinate tissues were homogenized and viral load was determined by real-time reverse-transcription polymerase chain reaction (RT-qPCR) as described previously [21, 22]. Infectious viral titer was determined by plaque assay in Vero E6 and MDCK cells, respectively [23, 24].

### Histopathology, Immunohistochemistry, and Immunofluorescence Staining

Formalin-fixed and paraffin-embedded lung, nasal turbinate, and small intestine tissues were cut into 4-µm tissue sections and stained with hematoxylin and eosin for histopathological examination. To differentiate the severity of lung tissue damage, each category of the histopathology changes for alveolitis including pulmonary edema, alveolar infiltration, and blood vessel inflammation were assessed and scored 0–4 as described previously (Supplementary Table 1) [25, 26]. Viral antigens were stained by immunohistochemistry or immunofluorescence with specific antibodies: rabbit anti-SARS-CoV-2 nucleocapsid (N) antibody or mouse anti-influenza A nucleoprotein (NP) antibody [27–29].

### Cytokine/Chemokine Profiling

Total RNA extracted from lung and nasal turbinate tissues was reverse transcribed into cDNA with MiniBEST Universal RNA Extraction Kit (Takara) and PrimeScriptTM RT reagent kit (Takara). RT-qPCR was performed with gene-specific primers (Supplementary Table 2) using SYBR Premix Ex Taq II Kit

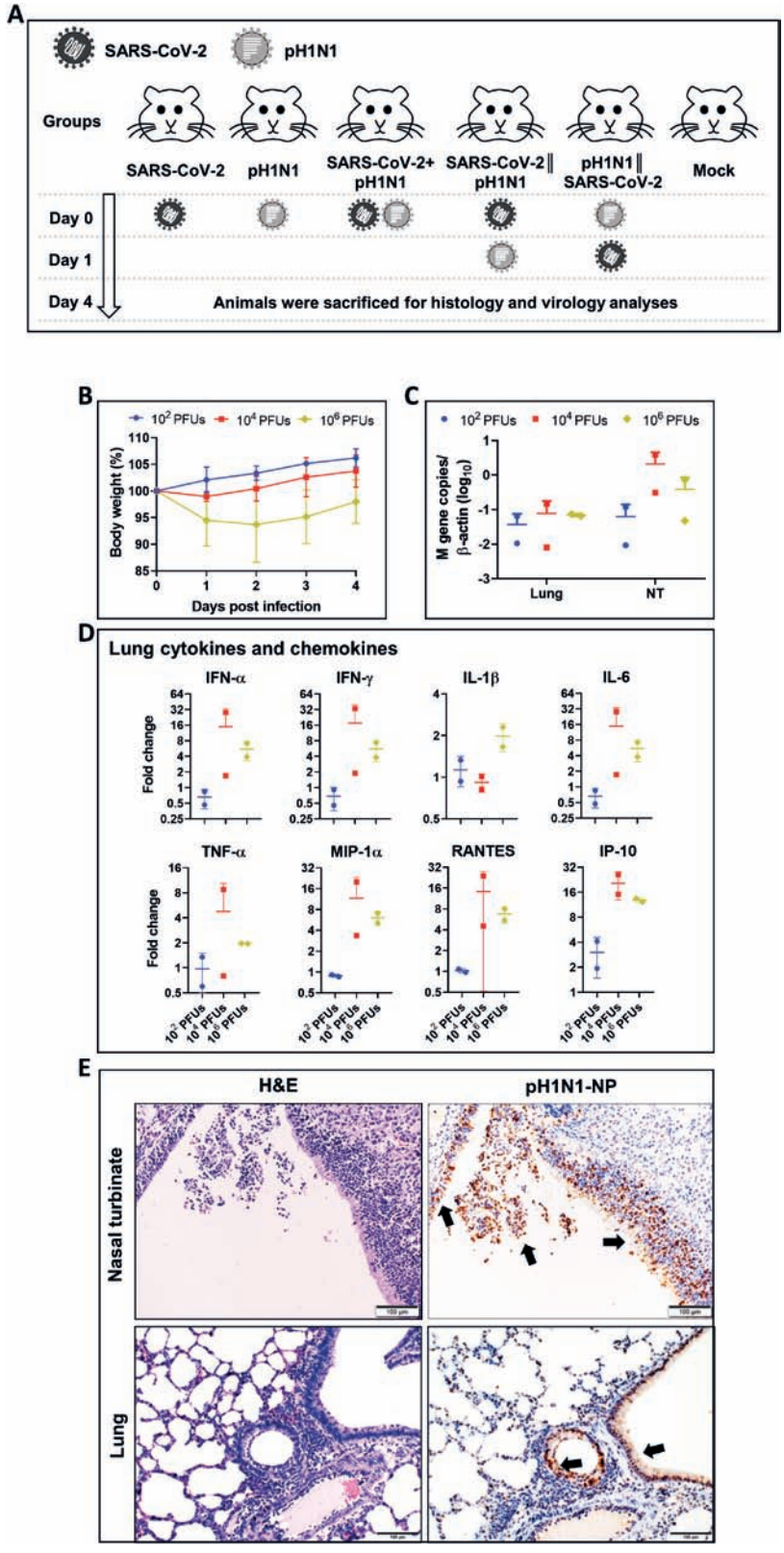


**Figure 1.** Schema for all hamster experiments and titration of A(H1N1)pdm09 virus inoculum for hamster infection. *A*, Schematic diagram for experimental layout. Six- to 8-week-old Syrian hamsters were grouped randomly; severe acute respiratory syndrome coronavirus 2 (SARS-CoV-2) and A(H1N1)pdm09 mouse-adapted A/Hong Kong 415742/2009 strain (pH1N1) were inoculated via the intranasal route. The animals were observed daily for disease signs and body weight change, and killed at 4 days postinfection (dpi) for virologic, cytokine/chemokine expression, and histopathological studies. *B*, Body weight changes during the 5-day experimental period for groups of animals inoculated with $10^2$, $10^4$, or $10^6$ plaque-forming units (PFUs) of pH1N1 alone. Weight on day 0 before virus inoculation was taken as 100%. *C*, Viral load determined

(Takara). The expression of cytokine/chemokine genes was analyzed by ΔΔCt method. Mock-infected tissue samples were used as baseline.

#### Microneutralization Antibody Assay

Neutralizing antibody titers against SARS-CoV-2 and A(H1N1)pdm09 in serum taken at 7 dpi and 14 dpi were determined by microneutralization assay in Vero E6 and MDCK cells as previously described [26, 30].

#### Statistical Analysis

All data were analyzed with GraphPad Prism 8.0 software. Student *t* test and one-way analysis of variance were used to determine significant differences among different groups. $P < .05$ was considered statistically significant.

## RESULTS

#### A(H1N1)pdm09 Pneumonia in Golden Syrian Hamsters

To find the optimal virus inoculum to induce pneumonia, we challenged hamsters by intranasal inoculation with $10^2$, $10^4$, or $10^6$ PFUs of mouse-adapted A(H1N1)pdm09. Only animals receiving $10^6$ PFUs inoculum lost 6.3% of body weight at 2 dpi (Figure 1B). Though their lung viral load at 4 dpi correlated with the dose of inocula (Figure 1C), there were no significant differences. Higher inoculum with $10^4$ or $10^6$ PFUs upregulated innate immune gene expression in the lungs which included interferon-α, interferon-γ, interleukin 1β (IL-1β), interleukin 6 (IL-6), tumor necrosis factor–α (TNF-α), macrophage inflammatory protein 1α (MIP-1α), regulated upon activation normal T-cell expressed protein (RANTES), and interferon-γ induced protein 10 (IP-10) (Figure 1D). Histologically, the lung tissue showed localized peribronchiolar and perivascular infiltration. The size and severity of affected lung area correlated with the dose of virus inoculum. But even the highest inoculum of $10^6$ PFUs did not cause conspicuous alveolar space infiltration or exudation (Figure 1E). Immunohistochemical staining for influenza virus nucleoprotein demonstrated extensive antigen expression in the nasal turbinate, trachea, bronchi, and bronchioles which were found, but much less frequently, in the pulmonary alveolar epithelium (Figure 1E).

#### Coinfection by High-Dose SARS-CoV-2 and A(H1N1)pdm09 Caused Severe Disease in Hamsters

To understand the impact of coinfection, we challenged hamsters intranasally with an inoculum of SARS-CoV-2 ($10^3$ PFUs) and A(H1N1)pdm09 ($10^5$ PFUs) mixed together, with SARS-CoV-2 ($10^3$ PFUs) alone, or with A(H1N1)pdm09 ($10^5$ PFUs) alone, respectively, as controls. Coinfected hamsters showed a maximum weight loss of 12.5% at 4 dpi compared with 8.4% in SARS-CoV-2 monoinfection and 7% in A(H1N1)pdm09 monoinfection, but the differences were not significant (Figure 2A). Coinfected animals showed signs of disease at 3 dpi with a significantly higher clinical score at 4 dpi (Figure 2B). Except for the lung infectious virus titer of SARS-CoV-2, which was significantly higher in SARS-CoV-2 monoinfection than coinfection, no significant difference in viral load or infectious virus titer for either A(H1N1)pdm09 or SARS-CoV-2 was found in other groups (Figure 2C and 2D). Similar degree of severe pulmonary alveolitis was observed in high-dose coinfected or $10^3$ PFUs SARS-CoV-2 monoinfected animals (Figure 2E).

#### Coinfection by Lower Doses of SARS-CoV-2 and A(H1N1)pdm09 Enhanced Lung Damage

To allow better differentiation of the effects of virus coinfection, the inoculum dose was reduced to SARS-CoV-2 (10 PFUs) and A(H1N1)pdm09 ($10^4$ PFUs) given by simultaneous or sequential challenge and compared with controls of monoinfection using the same dose of inoculum (Figure 1A). While animal challenged by A(H1N1)pdm09 monoinfection did not cause weight loss, SARS-CoV-2 monoinfection caused 5.8%, and the coinfection caused 9.6% of weight loss at 4 dpi (Figure 3A), with no significant differences in clinical scores among different groups (Figure 3B). Histopathological examination of coinfected animals at 4 dpi showed extensive and conspicuous pulmonary alveolar exudation (Figure 3C). The histology score in terms of pulmonary edema, inflammatory cell infiltration, and vasculitis were higher in coinfected animals than the single virus–infected animals (Figure 3D). Sequential inoculation of SARS-CoV-2 and A(H1N1)pdm09, 24 hours apart, also caused severe pulmonary alveolitis (Figure 3H, left and middle), which was comparable to $10^3$ PFU (high dose) SARS-CoV-2 infection (Figure 3H, right).

#### Viral Replication Profile in the Lung and Nasal Turbinate Tissue With Monoinfection, Simultaneous Coinfection, or Sequential Coinfections by Low-Dose Virus Inoculum

Although there was a time difference of 24 hours in the duration of challenge by the second virus in sequential coinfection when compared with simultaneous coinfection (Figure 1A), comparison

by real-time reverse-transcription polymerase chain reaction (RT-qPCR) for influenza A matrix gene (M gene) in homogenized lung and nasal turbinate (NT) tissues taken at 4 dpi. Data are presented as copies of M gene/copy of β-actin in log scale. *D*, Relative expression levels of inflammatory cytokine/chemokine messenger RNA determined by RT-qPCR in pH1N1-infected hamster lungs. Gene expression levels in mock control hamster lung tissues were used as baseline control. *E*, Representative histologic images of hamster NT (top panels) and lung tissues (bottom panels) at 4 dpi. NT tissue showed epithelial cell detachment in hematoxylin and eosin (H&E) image; the immunohistochemistry-stained pH1N1 nucleoprotein (NP) was abundantly expressed in epithelium and detached cells (brown color, arrows). The H&E images of lung tissue show peribronchiolar and perivascular inflammatory cell infiltration and bronchiolar epithelium cell death, and pH1N1 NP expression in the bronchiolar epithelial cells (arrows). Cytokine/chemokine abbreviations: IFN, interferon; IL, interleukin; IP-10, interferon-γ induced protein 10; MIP-1α, macrophage inflammatory protein 1 alpha; RANTES, regulated upon activation normal T-cell expressed protein; TNF-α, tumor necrosis factor alpha.

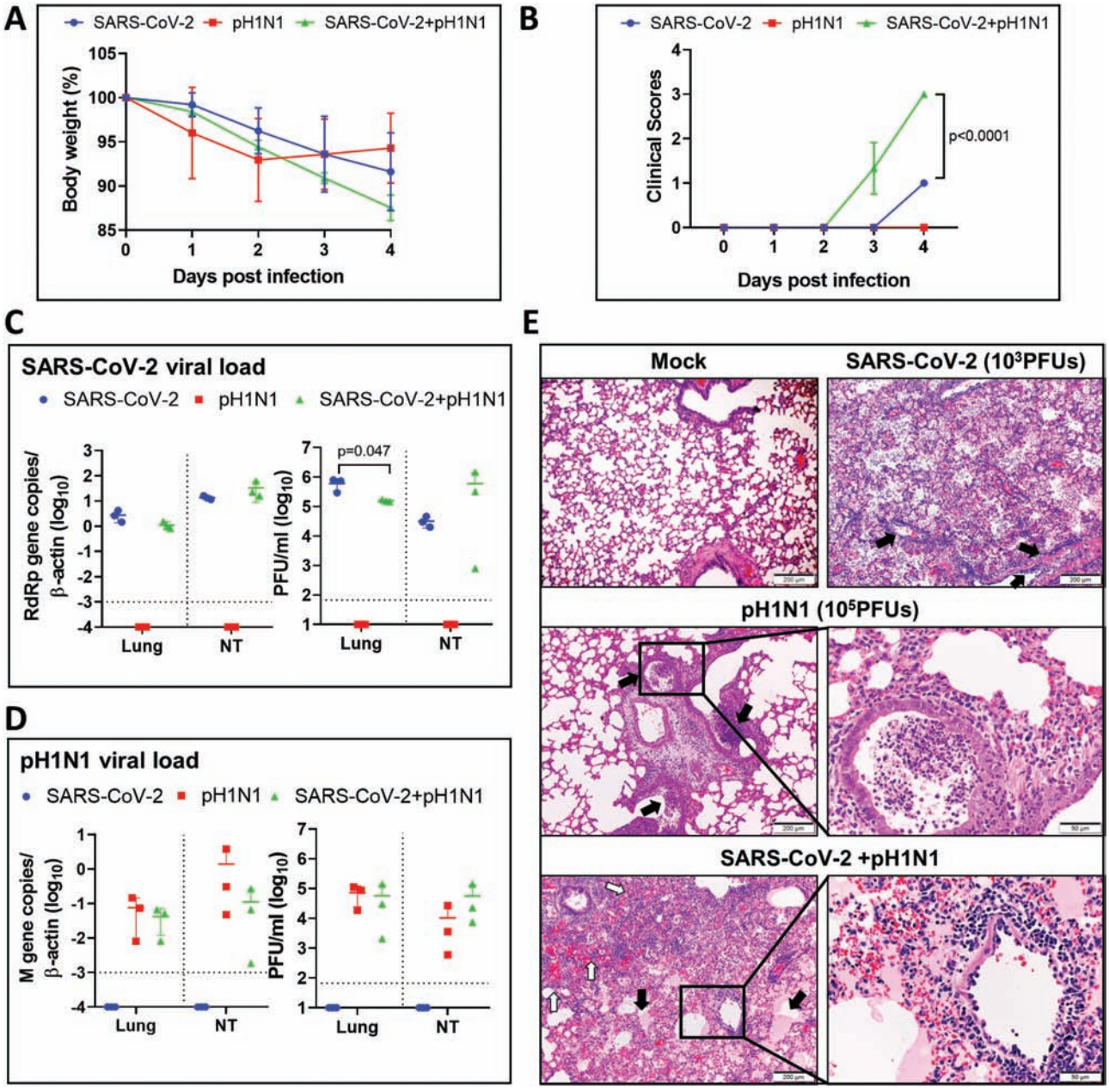


**Figure 2.** Simultaneous coinfection of hamsters by higher doses of severe acute respiratory syndrome coronavirus 2 (SARS-CoV-2) and mouse-adapted A/Hongkong/415742/2009 H1N1 (pH1N1). Groups of hamsters were intranasally inoculated with 50 μL of SARS-CoV-2 ($10^3$ plaque-forming units [PFUs]) and pH1N1 ($10^5$ PFUs) mixture; the animals were monitored for body weight and clinical sign scores, and killed at 4 days postinfection (dpi). Monoinfection by either viruses were included as controls. *A*, Body weight changes during the 5-day experimental period. Weight on day 0 before virus inoculation was taken as 100%. n = 3 each group. Error bars indicate mean ± standard deviation. *B*, Average clinical scores for disease signs including lethargy, ruffled fur, hunchback posture, and rapid breathing. A score of 1 was given to each of these clinical signs. *P* value was calculated by 2-way analysis of variance. *C*, SARS-CoV-2 viral load in homogenized lung or nasal turbinate (NT) tissues at 4 dpi after monoinfection or coinfection. Right panels are SARS-CoV-2 RdRp gene copies determined by real-time reverse-transcription polymerase chain reaction (RT-qPCR). The left panels are infectious viral titers determined by plaque assays in Vero E6 cells. *P* value was calculated by Student *t* test. Horizontal dashed line indicates detection limit of the assays. *D*, pH1N1 viral load in lung and nasal turbinate (NT) by RT-qPCR (right panel), or plaque assays in Madin-Darby canine kidney cells (left panel). Horizontal dashed line indicates detection limit of the assays. *E*, Representative images of lung histopathological changes at 4 dpi after monoinfection or coinfection. Top left image shows the normal lung structure of mock control. SARS-CoV-2 ($10^3$ PFUs) monoinfection showed diffuse alveolitis with massive alveolar space inflammatory cell infiltration, exudation, and pulmonary vasculitis (arrows, top right image). pH1N1 ($10^5$ PFUs)–infected lung showed conspicuous bronchiolar luminal cell debris (arrows), mild peribronchiolar infiltration, and perivascular edema; a bronchiole section inside the boxed area filled with cell debris is shown in magnified image. Images in the bottom panels are SARS-CoV-2+pH1N1-coinfected lung tissue, which showed massive exudation of protein-rich fluid (pink color) filling alveolar space (solid arrows), and a large area of alveolar hemorrhage (open arrows). Boxed area is magnified showing endotheliitis in a blood vessel.

of these findings are still relevant in understanding the virus interactions during coinfections at 4 dpi. In terms of SARS-CoV-2 replication, sequential coinfection with SARS-CoV-2 prior to A(H1N1)pdm09 had the highest lung viral load at 4 dpi. Simultaneous coinfection or sequential coinfection with A(H1N1)pdm09 prior to SARS-CoV-2 had a lower SARS-CoV-2 titer or

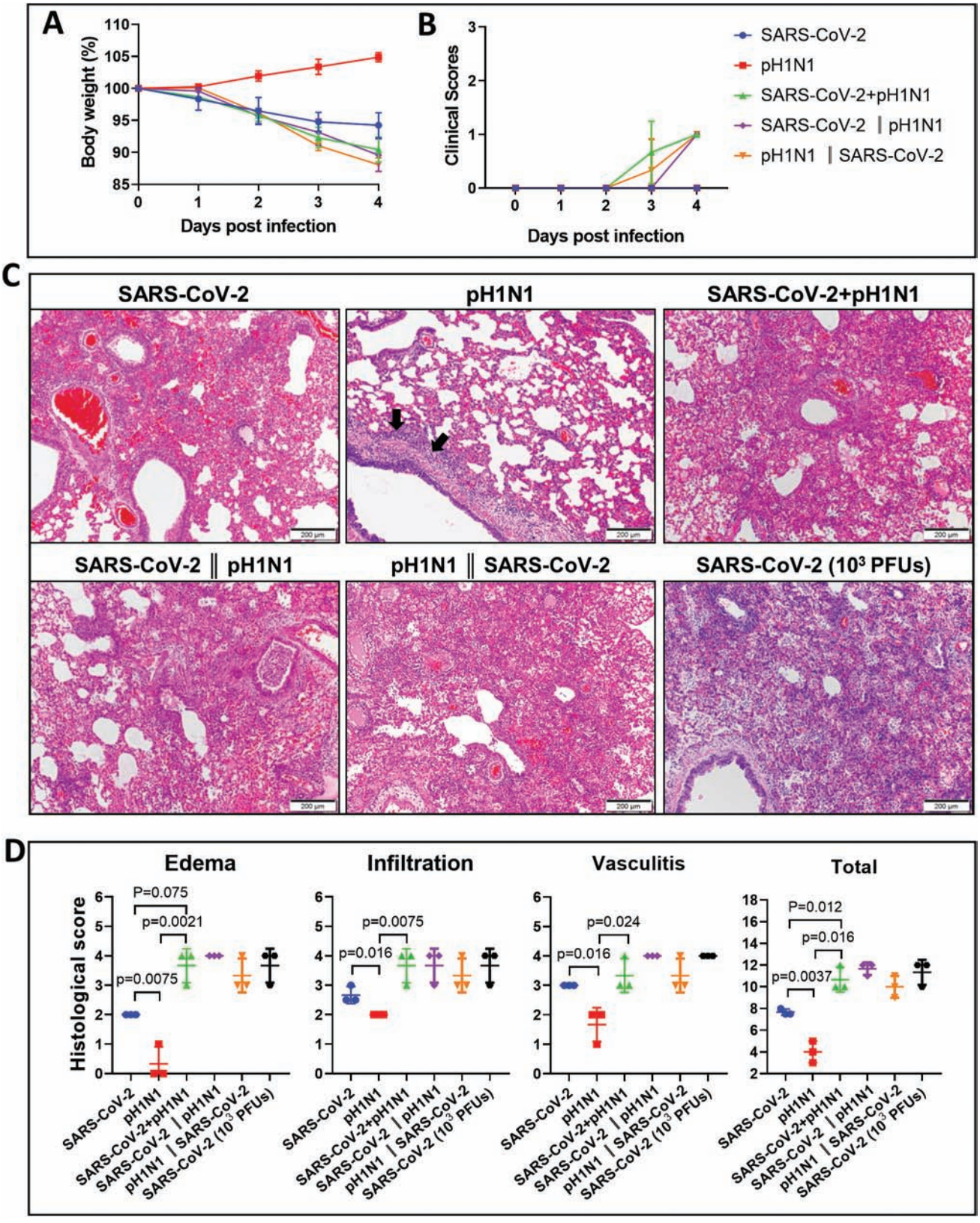


**Figure 3.** Simultaneous or sequential coinfections with lower doses of mouse-adapted A/Hongkong/415742/2009 H1N1 (pH1N1) and severe acute respiratory syndrome coronavirus 2 (SARS-CoV-2) in hamsters showed increased disease severity. Groups of hamsters were inoculated with SARS-CoV-2 (10 plaque-forming units [PFUs]) and pH1N1($10^4$ PFUs), singly, simultaneously, or sequentially as described in Figure 1A. *A*, Body weight changes during the 5-day experimental period. n = 3 each group. Error bars indicate mean ± standard deviation (SD). *B*, Average clinical scores for signs of disease including lethargy, ruffled fur, hunchback posture, and rapid breathing. A score of 1 was given to each of these clinical signs. *C*, Representative hematoxylin and eosin stained images of the lungs at 4 days postinfection (dpi) after monoinfection simultaneous,

viral load than with SARS-CoV-2 monoinfected (Figure 4A). In terms of A(H1N1)pdm09 replication, A(H1N1)pdm09 inoculation prior to SARS-CoV-2 had the highest lung A(H1N1)pdm09 viral load but not the infectious titer (Figure 4B).

Immunohistochemical staining for the intensity of SARS-CoV-2 N antigen expression at 4 dpi appeared correlative with the lung SARS-CoV-2 viral loads, which was highest with sequential coinfection [SARS-CoV-2 prior to A(H1N1)pdm09], followed by SARS-CoV-2 monoinfected, and then sequential coinfection [A(H1N1)pdm09 prior to SARS-CoV-2] (Figure 4C). Double immunofluorescent antigen staining for SARS-CoV-2 N and A(H1N1)pdm09 NP antigens rarely showed co-localization in cells from lungs of coinfected animals (Figure 4D and 4E). Overall, the amount of cells with SARS-CoV-2 N expression was higher than the amount of cells with A(H1N1)pdm09 NP expression in coinfected animals. While inflammatory cytokine/chemokine gene expressions in lung tissues after sequential coinfection with SARS-CoV-2 prior to A(H1N1)pdm09 were higher than the other groups, they were generally not significantly different except for IL-1β in SARS-CoV-2 monoinfection group (Figure 4F).

Though viral loads in the lung and nasal turbinate tissues of SARS-CoV-2 monoinfection or coinfection groups were similar at 7 dpi and 14 dpi (Figure 4G), infectious virus titer was not detectable by plaque assays, which may be related to mounting of antibody response (data not shown). SARS-CoV-2 shedding by virus titer assay in oral swabs after monoinfection or simultaneous coinfection was similar during 2 dpi to 8 dpi. Only simultaneous coinfection group continued to shed SARS-CoV-2 till 10 dpi (Figure 4H, left). Oral swabs for A(H1N1)pdm09 virus titer were higher in coinfected hamsters at 2, 4, and 6 dpi, but not significantly different from monoinfection (Figure 4H, right).

As for extrapulmonary pathology, increased intestinal inflammatory infiltration and edema were observed in coinfected animals at 4 dpi (Figure 5A). In the intestinal sections, SARS-CoV-2 N antigen–expressing enterocytes were more easily seen in coinfected hamsters than in SARS-CoV-2 monoinfection by immunofluorescence (Figure 5B). However, no A(H1N1)pdm09 NP antigen was detected from intestinal sections.

#### Delayed Serum Antibody Response Associated With Delayed Resolution of Lung Inflammation in Coinfected Hamsters

Unlike single virus–infected animals, lung tissues of animals simultaneously coinfected with 10 PFUs of SARS-CoV-2 and $10^4$ PFUs of A(H1N1)pdm09 still showed alveolar inflammatory cell infiltration, bronchiolar luminal exudation, and frequently perivascular inflammatory cell infiltration at 7 and 14 dpi (Figure 6A). Notably, these coinfected hamsters had significantly lower titer of serum neutralizing antibody against SARS-CoV-2 at 7 dpi (mean, 33.3) compared with SARS-CoV-2 monoinfection (mean, 160) (Figure 6B). Serum neutralizing antibody titer against A(H1N1)pdm09 was slightly lower in coinfected animals than A(H1N1)pdm09 monoinfected at 7 and 14 dpi, but not significantly different (Figure 6C). The clinical score, maximal weight loss, histology score, virologic profile, antigen expression and neutralizing antibody titers in different groups of monoinfected or coinfected hamsters are summarized in Table 1.

## DISCUSSION

In this study, we confirmed that hamsters are susceptible to mouse-adapted A(H1N1)pdm09 [18] and human isolate of SARS-CoV-2 [16]. Moreover, hamsters appeared to be more susceptible to SARS-CoV-2 with a lower inoculum dose but had more weight loss (Table 1). Our hamster coinfection model with SARS-CoV-2 and A(H1N1)pdm09 suggested that simultaneous or sequential coinfection can induce more severe tissue damage than monoinfection. In sequential coinfection with SARS-CoV-2 prior to A(H1N1)pdm09, SARS-CoV-2 dominated over A(H1N1)pdm09 with higher viral load, histology score, and cytokine/chemokine gene expressions than monoinfection by SARS-CoV-2 or A(H1N1)pdm09. However, sequential coinfection with A(H1N1)pdm09 prior to SARS-CoV-2 exposure resulted in lower lung SARS-CoV-2 viral load than the SARS-CoV-2 monoinfection despite similar degree of lung inflammatory damage in coinfections. Moreover, the lung A(H1N1)pdm09 viral load of sequential coinfection by A(H1N1)pdm09 prior to SARS-CoV-2 exposure was significantly higher than in other groups. Notably, nasal turbinate SARS-CoV-2 titer and lung A(H1N1)pdm09 viral load were also higher in sequential coinfection with prior A(H1N1)pdm09 infection. These findings suggested that while hamsters are generally more susceptible to SARS-CoV-2 than A(H1N1)pdm09, even in simultaneous coinfection, both viral load and infectious titer of SARS-CoV-2 were lower than that of SARS-CoV-2 monoinfection. Thus, coinfection by A(H1N1)pdm09 may likely interfere with SARS-CoV-2 replication in the lung and most prominently when there is prior A(H1N1)pdm09 infection. However, such viral interference does not

and sequential coinfections. Lung sections of SARS-CoV-2 (10 PFUs) monoinfection showed patchily distributed alveolar wall and alveolar space infiltration. pH1N1($10^4$ PFUs)–infected lung showed peribronchiolar infiltration, bronchiolar wall infiltration (arrows), and alveolar wall congestion. The images for the lung of both simultaneous and sequential coinfections showed diffuse alveolar infiltration, severe exudation, and alveolar hemorrhage. The severity of damage is much greater when compared to either virus monoinfection, but is comparable to higher dose of SARS-CoV-2 ($10^3$ PFUs) monoinfection shown in the lower right image. *D*, Histology scores for the lung sections at 4 dpi after monoinfection or coinfections. Each category of the characteristic histopathology changes for alveolitis caused by virus infection, including pulmonary edema, alveolar infiltration, and blood vessel inflammation were examined and scored. Lung sections from higher dose SARS-CoV-2 ($10^3$ PFUs) monoinfection were included for comparison. n = 3 each group. Three lung lobes were examined from each hamster. *P* value was calculated by one-way analysis of variance. Error bars indicate mean ± SD. Double vertical lines indicate sequential inoculation (24 hours apart); + indicates simultaneous inoculation.

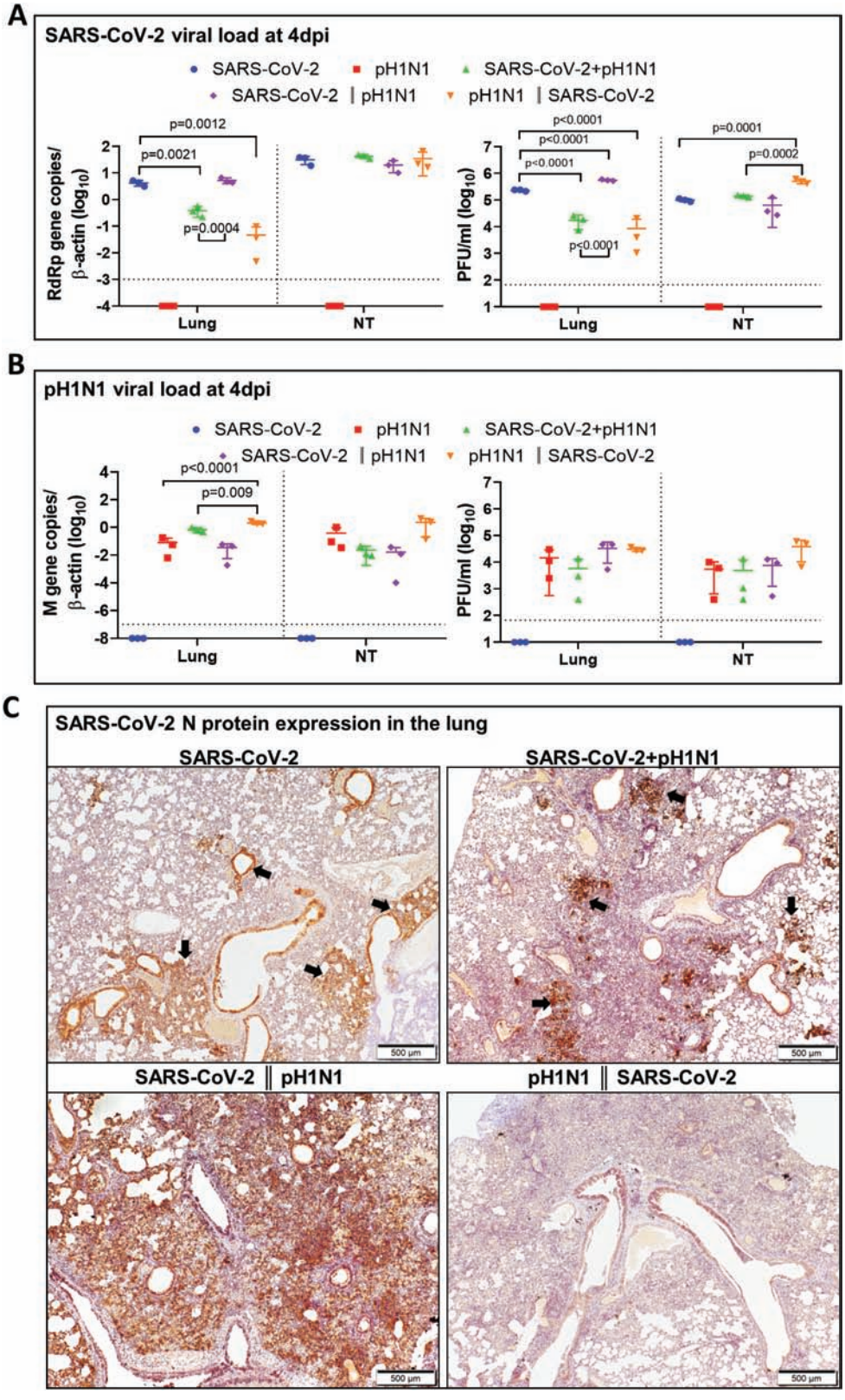


**Figure 4.** Viral replication profiles in the lung and nasal turbinate (NT) tissue of hamsters after monoinfection, simultaneous, or sequential coinfection. *A*, Severe acute respiratory syndrome coronavirus 2 (SARS-CoV-2) viral load in lung and NT tissues. SARS-CoV-2 RdRp gene copies determined by real-time reverse-transcription polymerase chain reaction (RT-qPCR) (left panel). SARS-CoV-2 infectious viral titers were determined by plaque assays in Vero E6 cells (right). n = 3 each group. *P* values are calculated by one-way analysis of variance (ANOVA). Error bars indicate mean ± standard deviation (SD). Horizontal dashed line indicates detection limit of the assays. *B*, Mouse-adapted A/Hongkong/415742/2009 H1N1 (pH1N1) viral load in lung and NT tissues by RT-qPCR (influenza A matrix gene, left panel) or plaque assays in Madin-Darby canine kidney cells (right). n = 3 each group. *P* values are calculated by one-way ANOVA. Error bars indicate mean ± SD. Horizontal dashed line indicates detection limit of the assays. *C*, Representative images of immunohistochemistry-stained SARS-CoV-2 N protein in the lung tissues after monoinfection or coinfection. SARS-CoV-2 N protein

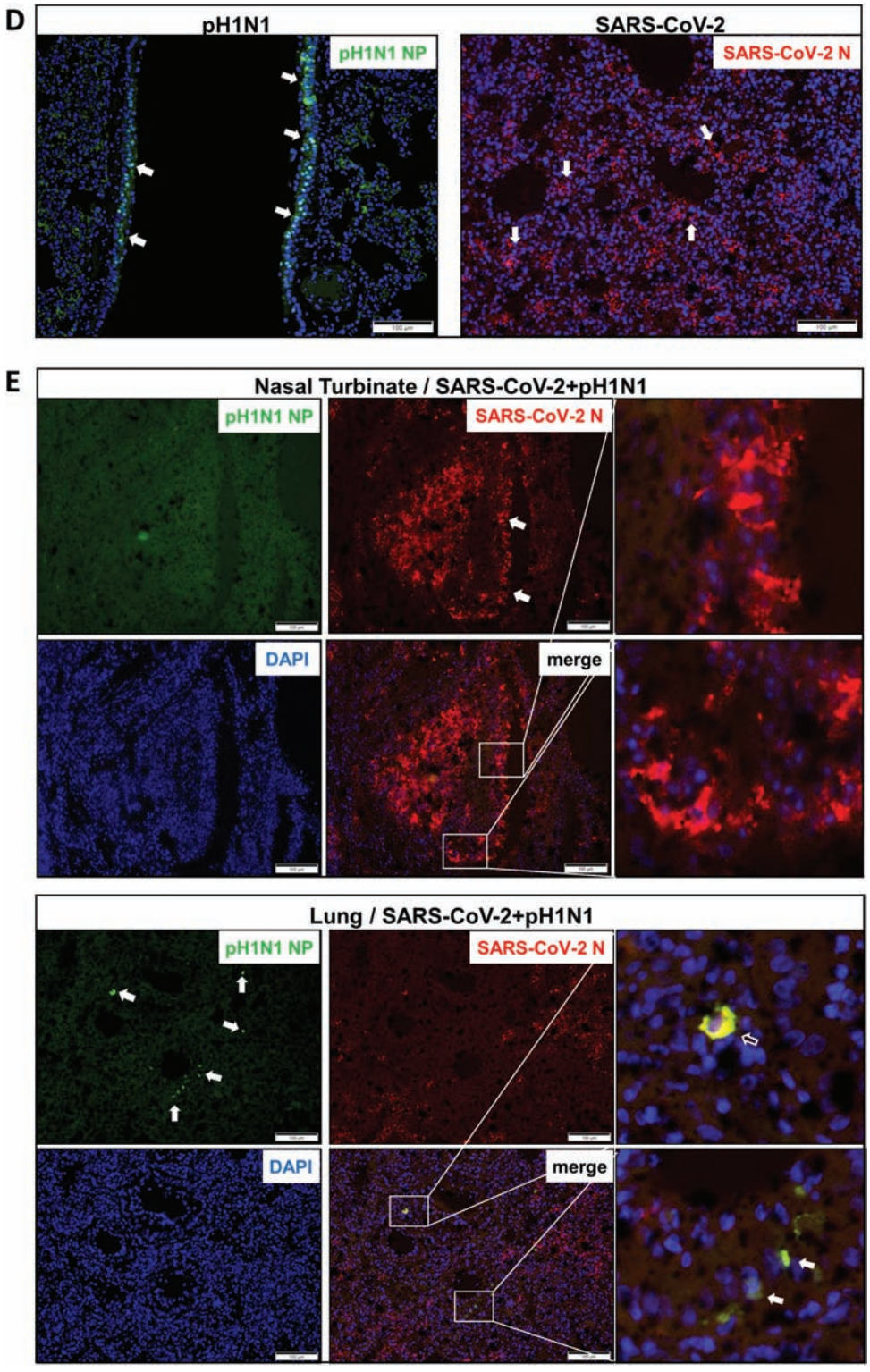


**Figure 4.** Continued.

was stained in brown. The images of SARS-CoV-2 monoinfection shows N protein expression in regional alveoli and bronchiolar epithelium (arrows); simultaneously coinfected lung has small patches of N protein expression in a large area of inflammatory consolidated lung tissue (arrows); the lung coinfected sequentially by SARS-CoV-2 prior to pH1N1 (SARS-CoV-2 || pH1N1) shows extensive N protein expression distributed diffusely in the lung, whereas in sequential coinfection by pH1N1 prior to SARS-CoV-2 (pH1N1 || SARS-CoV-2), the large area of inflammatory consolidation in lung tissue shows a few N protein–positive cells. *D*, Immunofluorescence images illustrate pH1N1 NP antigen and SARS-CoV-2 N antigen in single virus–infected hamster lung tissues. pH1N1 nucleoprotein (NP) is only seen in the epithelium of bronchiolar epithelium, not in alveoli (NP, green). SARS-CoV-2 N antigen is seen diffusely distributed in alveoli (N, red). *E*, Dual immunofluorescence images illustrate the distribution of pH1N1 NP and SARS-CoV-2 N in simultaneously coinfected hamster NT (upper panels) and lung tissues (lower panels). pH1N1 NP antigen was rarely seen in the coinfected NT tissues, whereas

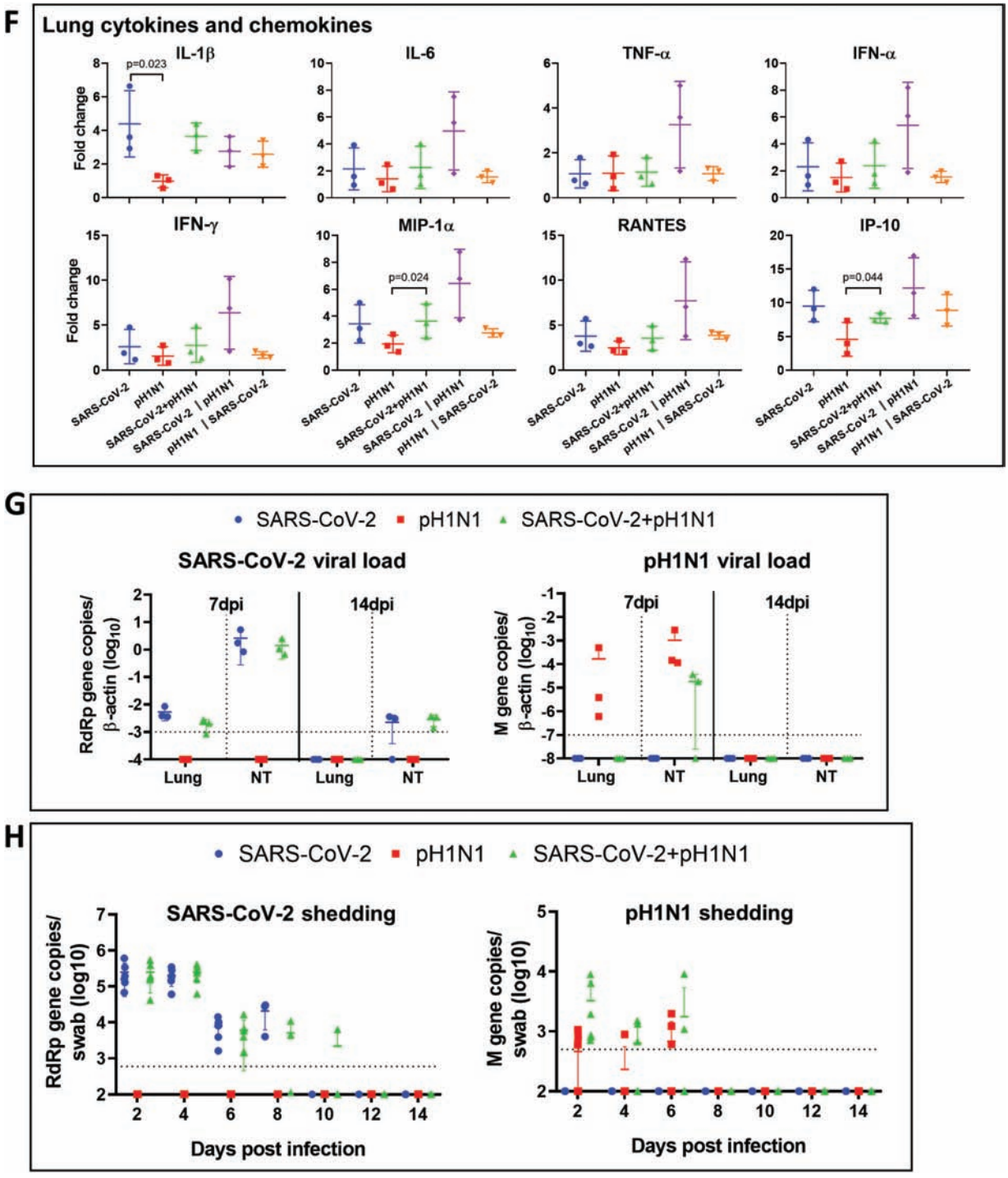


**Figure 4.** Continued.

SARS-CoV-2 N protein was abundantly detected (arrows, N stained red). In the lung tissue, the 2 viral antigens also distributed differently. These images show pH1N1 NP expression in a few cells in the bronchiolar epithelium, but not in alveoli (arrows, green), while SARS-CoV-2 N is seen in alveoli (red) but not in bronchiole. Co-localization of SARS-CoV-2 N and pH1N1 NP antigen is shown in a macrophage (magnified image, open arrow). *F*, Relative expression of inflammatory cytokines/chemokines in hamster lung tissues determined by RT-qPCR using gene-specific primers. *G*, RT-qPCR determined SARS-CoV-2 viral load (left) and pH1N1 viral load (right) in the lung and NT tissues taken at 7 days postinfection (dpi) or 14 dpi after simultaneous coinfection or monoinfection. n = 3 each group. Error bars indicate mean ± SD. Horizontal dashed line indicates detection limit of the assays. *H*, SARS-CoV-2 (left) and pH1N1 (right) virus shedding from oral swabs determined by RT-qPCR. Oral swab samples were collected every other day during the 14 days after virus challenge. Error bars indicate mean ± SD. Horizontal dashed line indicates detection limit of the assays. Double vertical lines indicate sequential inoculation (24 hours apart); + indicates simultaneous inoculation. Abbreviations: IP-10, interferon-γ induced protein 10; M gene, influenza A matrix gene; MIP-1α, macrophage inflammatory protein 1 alpha; N, severe acute respiratory syndrome coronavirus 2 nucleocapsid protein; NP, influenza A nucleoprotein; NT, nasal turbinate; pH1N1, mouse-adapted A/Hongkong/415742/2009 H1N1; PFU, plaque-forming unit; RANTES, regulated upon activation, normal T-cell expressed protein; RdRp, RNA-dependent RNA polymerase; SARS-CoV-2, severe acute respiratory syndrome coronavirus 2; TNF-α, tumor necrosis factor alpha.

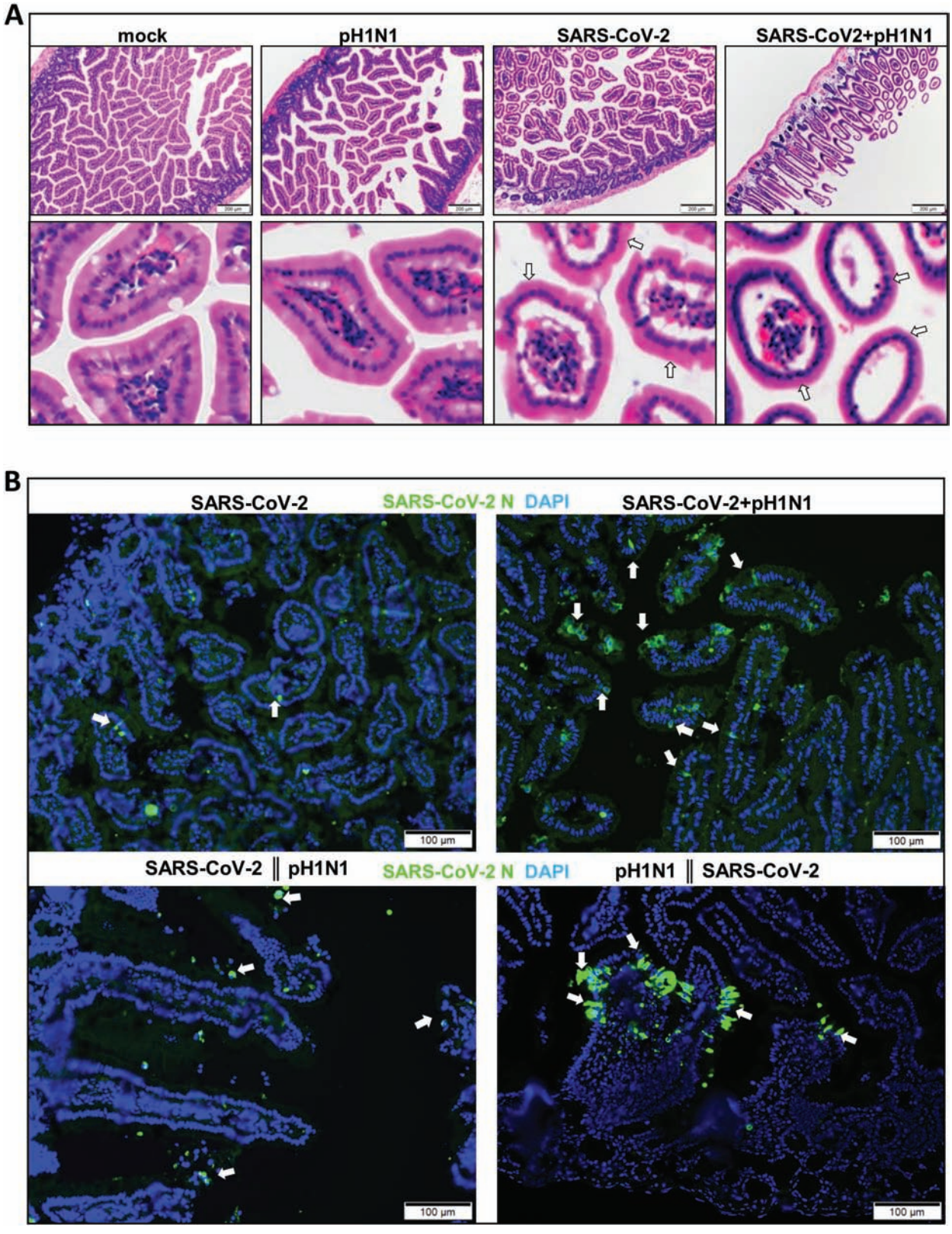


**Figure 5.** Simultaneous severe acute respiratory syndrome coronavirus 2 (SARS-CoV-2) and mouse-adapted A/Hongkong/415742/2009 H1N1 (pH1N1) coinfection induced intestinal tissue damage. *A*, Hematoxylin and eosin images of small intestine sections after monoinfection or simultaneous coinfection of hamsters at 4 days postinfection. Normal structure of intestinal villi is shown in mock control hamster. No obvious morphological changes are shown in pH1N1 ($10^4$ plaque-forming units [PFUs]) SARS-CoV-2 (10 PFUs) caused some degree of intestinal villi edema (arrows), but simultaneous coinfection increased small intestine inflammatory infiltration and intestinal villi edema, which cause deformation of villi (arrows). *B*, Images of immunofluorescence-stained SARS-CoV-2 N protein in intestinal sections. N protein was stained in green (arrows), cell nuclei in blue (DAPI). Double vertical lines indicate sequential inoculation (24 hours apart); + indicates simultaneous inoculation.

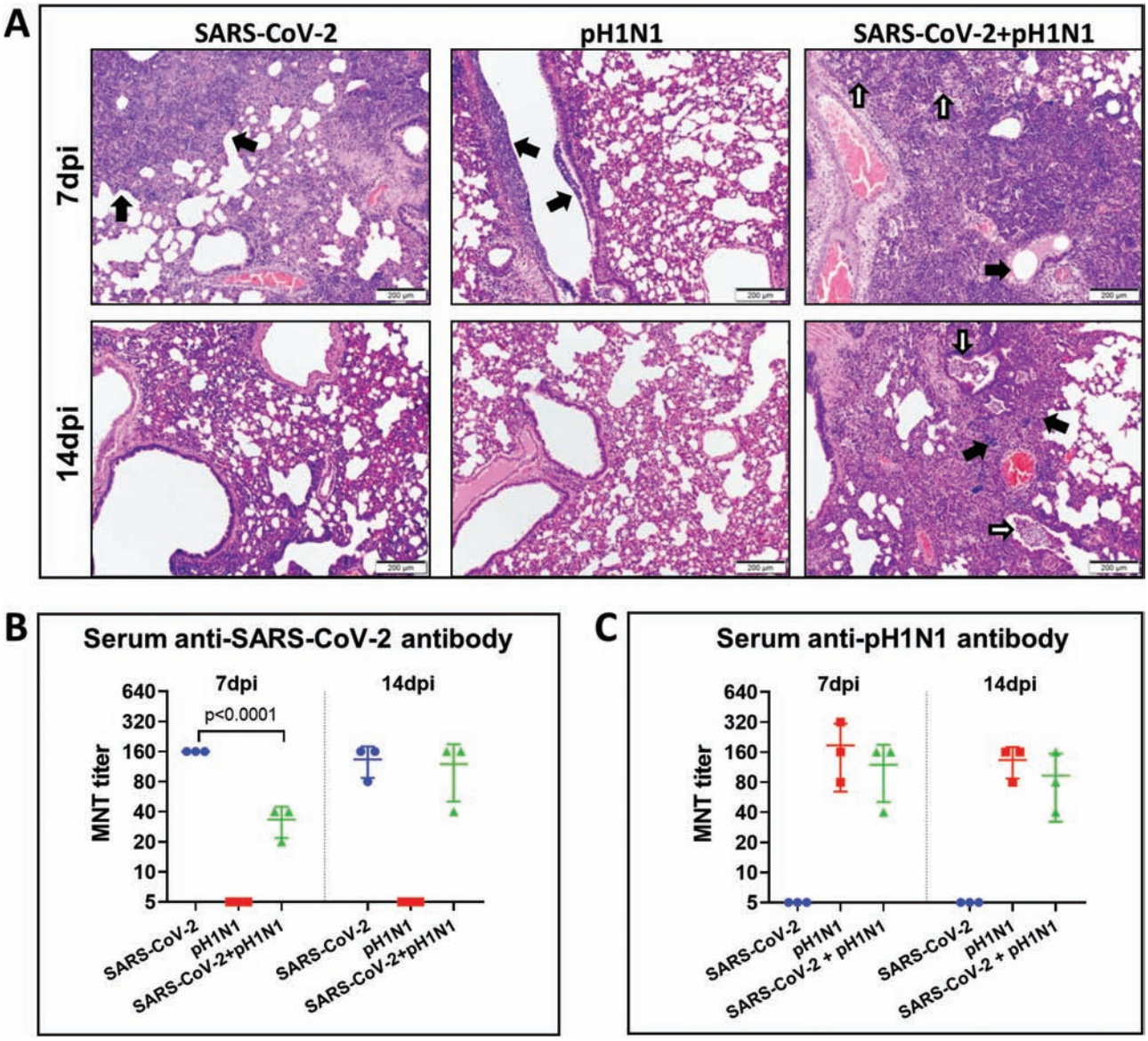


**Figure 6.** Reduced antibody responses and delayed resolution of lung inflammation after severe acute respiratory syndrome coronavirus 2 (SARS-CoV-2) and mouse-adapted A/Hongkong/415742/2009 H1N1 (pH1N1) coinfection in hamsters. *A*, Representative hematoxylin and eosin images of lung tissues at 7 days postinfection (dpi) (upper panel) and 14 dpi (lower panel) after monoinfection or simultaneous coinfection. At 7dpi, SARS-CoV-2 infected lung showed proliferative changes (black arrows); pH1N1 infected lung only showed bronchiolar luminal cell debris (black arrows); while the lung of coinfection showed alveolar infiltration (while arrows) and bronchiolar secretion (black arrow). At 14dpi, only the coinfected lung showed bronchiolar luminal infiltration (white arrows) and foci of alveolar infiltration (black arrows). *B*, Serum neutralizing antibodies against SARS-CoV-2 (left) and pH1N1 (right) were determined by microneutralization test (MNT) on Vero E6 cells and Madin-Darby canine kidney cells, respectively.

appear to lessen the degree of inflammatory damage to the lung. Simultaneous coinfection was associated with delay in the resolution of severe lung damage at 7 and 14 dpi, and these coinfected hamsters developed significantly lower titer of serum SARS-CoV-2 neutralizing antibody at 7 dpi than that of SARS-CoV-2 infection. SARS-CoV-2 shedding in oral swabs of coinfected hamsters was therefore longer than monoinfection.

The clinical significance of acute respiratory virus coinfections in terms of hospital stay, the need for intensive care, and mortality rate is controversial [31]. While data for adults are lacking, most studies suggested that the clinical severity is not different between children with single respiratory virus infection and virus coinfection, but the mortality is higher in preschool children [32]. The historically unprecedented co-circulation of SARS-CoV-2 and seasonal influenza poses a great challenge to our healthcare system in the 2020 winter. An epidemiological study showed that the risk of testing positive for SARS-CoV-2 was 68% lower among influenza-positive cases, which suggested possible interference or competition between these 2 viruses [13], while coinfection with both viruses had greater risk

**Table 1. Comparison Between Monoinfection and Coinfection With Severe Acute Respiratory Syndrome Coronavirus 2 and A(H1N1)pdm09 in a Hamster Model[a]**

| Characteristic | SARS-CoV-2 (10 PFUs) | pH1N1 ($10^4$ PFUs) | SARS-CoV-2 + pH1N1 | SARS-CoV-2 \|\| pH1N1 | pH1N1 \|\| SARS-CoV-2 |
|---|---|---|---|---|---|
| Overall severity | | | | | |
| Clinical score, mean ± SD[b] | 0.00 ± 0.00 | 0.00 ± 0.00 | 1.00 ± 0.00 | 1.00 ± 0.00 | 1.00 ± 0.00 |
| Body weight change, %, mean ± SD[c] | –5.77 ± 1.96 | 4.87 ± 0.71 | –9.57 ± 1.96 | –11.93 ± 1.08 | –10.43 ± 2.54 |
| Lung histology score | 7.60 ± 0.29 | 4.00 ± 0.58 | 10.67 ± 0.67** | 11.67 ± 0.58** | 10.00 ± 1.0** |
| Nasal turbinate virus replication | | | | | |
| SARS-CoV-2 gene copy, log copies/1 × 104 β-actin, mean ± SD | 5.48 ± 0.18 | … | 5.61 ± 0.08 | 5.25 ± 0.23 | 5.45 ± 0.32 |
| SARS-CoV-2 plaque, log PFU/mL, mean ± SD | 5.00 ± 0.06 | … | 5.14 ± 0.04 | 4.71 ± 0.35 | 5.70 ± 0.08***/### |
| pH1N1 gene copy, log copies/1 × 104 β-actin, mean ± SD | … | 3.17 ± 0.76 | 2.24 ± 0.38 | 1.56 ± 1.36 | 4.06 ± 0.80 |
| pH1N1 plaque, log PFU/mL, mean ± SD | … | 3.46 ± 0.75 | 3.25 ± 0.78 | 3.6 ± 0.76 | 4.43 ± 0.53 |
| Lung virus replication | | | | | |
| SARS-CoV-2 gene copy, log copies/1 × 104 β-actin, mean ± SD | 4.62 ± 0.11 | … | 3.55 ± 0.20** | 4.71 ± 0.10### | 2.41 ± 0.67** |
| SARS-CoV-2 plaque, log PFU/mL, mean ± SD | 5.36 ± 0.03 | … | 4.19 ± 0.29*** | 5.74 ± 0.03***/### | 3.65 ± 0.64*** |
| pH1N1 gene copy, log copies/1 × 104 β-actin, mean ± SD | … | 2.61 ± 0.73 | 3.82 ± 0.16 | 2.23 ± 0.83 | 4.32 ± 0.09 ***/### |
| pH1N1 plaque, log PFU/mL, mean ± SD | … | 3.98 ± 0.54 | 3.41 ± 0.77 | 4.36 ± 0.54 | 4.48 ± 0.07 |
| Lung antigen expression[d] | | | | | |
| SARS-CoV-2 nucleocapsid protein | ++ | … | ++ | +++ | + |
| pH1N1 nucleoprotein | … | + | + | + | + |
| Serum neutralizing antibody | | | | | |
| SARS-CoV-2 neutralizing titer at 7 dpi, mean ± SD | 160.0 ± 0.0 | <5 | 33.3 ± 11.6*** | ND | ND |
| SARS-CoV-2 neutralizing titer at 14 dpi, mean ± SD | 133.3 ± 46.2 | <5 | 120.0 ± 69.3 | ND | ND |
| pH1N1 neutralizing titer at 7 dpi, mean ± SD | <5 | 186.7 ± 122.2 | 120.0 ± 69.3 | ND | ND |
| pH1N1 neutralizing titer at 14 dpi, mean ± SD | <5 | 133.3 ± 46.2 | 93.3 ± 61.1 | ND | ND |

Abbreviations: dpi, days postinfection; ND, not determined; PFU, plaque-forming units; pH1N1, mouse-adapted A/Hongkong/415742/2009 H1N1; SARS-CoV-2, severe acute respiratory syndrome coronavirus 2; SD, standard deviation.

[a]All data represent 4 dpi unless otherwise indicated; || indicates sequential inoculation (24 hours apart).

[b]A score of 1 was given to each of the following clinical signs: lethargy, ruffled fur, hunchback posture, and rapid breathing.

[c]Body weight at 4 dpi minus 0 dpi body weight.

[d]+, a few antigen expressing cells; ++, patches of antigen expressing cell; +++, abundant antigen expressing cells diffuse distribution.

$^{**}P < .01$, $^{***}P < .001$ when compared to monoinfection of SARS-CoV-2 and pH1N1.

$^{###}P < .001$ when compared to SARS-CoV-2/pH1N1 coinfection.

of ventilator use, intensive care admission, and death [33]. Since controlling for the type of respiratory viruses, their relative dose, order of acquisition, route to the upper or lower airway, and the effect of viral interference in different age or comorbid patient groups was not clinically possible, we set up this hamster coinfection model to understand the significance of this potentially ominous interaction between a new emerging pandemic coronavirus and the presently circulating seasonal influenza A(H1N1)pdm09. Our findings are consistent with the epidemiological study in that the animal lung pathology was more severe with simultaneous or sequential coinfections. This finding is consistent with the previous report of more severe lung pathology in guinea pigs coinfected by 2003 SARS-CoV and reovirus isolated from a SARS patient [15]. Interestingly, infectious SARS-CoV-2 titer was also increased in nasal turbinate of hamsters with preceding A(H1N1)pdm09 inoculation, which is compatible with an epidemiological modeling study suggesting that SARS-CoV-2 transmission increased 2- to 2.5-fold due to coinfection with influenza [14]. Finally, the SARS-CoV-2 viral load was lower in the lungs of hamsters with preceding A(H1N1)pdm09 inoculation, suggesting that A(H1N1)pdm09 outcompeted SARS-CoV-2 in this setting.

Our previous study showed that resolution of inflammatory lung damage due to SARS-CoV-2 should be complete after 7 dpi [16]. The present study showed that the inflammatory damage due to A(H1N1)pdm09 was mild. Besides the severity of lung damage by coinfection and higher inflammatory cytokine/chemokine responses, we observed a delay of resolution of lung inflammation in coinfected hamsters even by 14 dpi. This was accompanied by a significantly lower neutralizing antibody titer against SARS-CoV-2 but not for A(H1N1)pdm09. Based on these findings of increased disease severity, delayed resolution and lung healing, and a blunted adaptive immune response, a high compliance to population-wide vaccination against seasonal influenza is warranted to prevent severe disease resulting from coinfection with SARS-CoV-2 as an effective antiviral against SARS-CoV-2 is still lacking or not readily available. Early detection of coinfection by multiplex RT-PCR could be important for early initiation of antivirals within 48 hours of symptom onset to improve the prognosis of patients with coinfection.

Viral interference is a phenomenon where one virus competitively suppresses the replication of another coinfecting virus, and is generally believed to down-modulate virus virulence, cell death, disease severity, and transmissibility [34]. In terms of acute respiratory virus coinfection animal model, a mouse model of coinfection by influenza A PR8 virus and rhinovirus or mouse hepatitis virus was reported to show an attenuation of disease severity when rhinovirus or mouse hepatitis virus was given 2 days prior to the influenza virus [35]. Similarly, another ferret study showed reduction of the severity of influenza if prior respiratory syncytial virus was given [36]. In our study, though A(H1N1)pdm09 appeared to interfere with SARS-CoV-2 replication, it actually increased the disease severity. Viral interference can be mediated by the innate immune interferon response, defective interfering particles, viral proteases and proteins, competition for cellular factors, and RNA interference. However the induction of interferon response by simultaneous or sequential A(H1N1) pdm09 infection may also augment the inflammatory cytokine storm associated with SARS-CoV-2 infection. The time gap between the inoculation of coinfecting viruses, their rate of replication, the dose of virus inoculum, and the host adaptive immune response are the other major factors that affect viral interference. Indeed, preceding A(H1N1)pdm09 inoculation appeared to interfere more with SARS-CoV-2 replication in our hamster model, and simultaneous coinfection suppressed the neutralizing antibody response against SARS-CoV-2.

Besides hamsters, human ACE2 transgenic mice, ferrets, and primates are possible options for developing laboratory animal models of coinfection as they are all susceptible to SARS-CoV-2 and influenza virus [37]. In terms of cost, availability, ease of manipulation, and simulation to human disease, the hamster model was chosen for this study. Our study has limitations due to the differences in the intrinsic susceptibility of hamsters to SARS-CoV-2 and A(H1N1)pdm09. While the laboratory hamsters are immunologically naive to both viruses, patients generally have some degree of immunity against seasonal influenza viruses. Our study only used A(H1N1)pdm09 but not influenza A(H3N2) or B viruses. A live attenuated mucosal seasonal influenza virus vaccine which also encodes the receptor binding domain of the Spike protein of SARS-CoV-2 should be investigated if SARS-CoV-2 becomes an antigenically drifting common cold virus [38]. More studies on these important unanswered questions are warranted.

## Supplementary Data

Supplementary materials are available at *Clinical Infectious Diseases* online. Consisting of data provided by the authors to benefit the reader, the posted materials are not copyedited and are the sole responsibility of the authors, so questions or comments should be addressed to the corresponding author.

## Notes

***Author contributions.*** A. J. Z., A. C.-Y. L., J. F.-W. C., and K.-Y. Y. had roles in the study design, data collection, data analysis, data interpretation, and writing of the manuscript. F. L., C. L., Y. C., H. C., S.-Y. L., P. W., C. C.-S. C., V. K.-M. P., S. F., K. K.-W. T., and H. C. had roles in the experiments, data collection, data analysis. All authors reviewed and approved the final version of the manuscript.

***Disclaimer.*** The funding sources had no role in the study design, data collection, analysis, interpretation, or writing of the report.

***Financial support.*** This work was partly supported by funding from the National Program on Key Research Project of China (grant numbers 2020YFA0707500 and 2020YFA0707504); the Consultancy Service for Enhancing Laboratory Surveillance of Emerging Infectious Diseases and Research Capability on Antimicrobial Resistance, Department of Health, the Hong Kong Special Administrative Region Government; High Level-Hospital Program, Health Commission of Guangdong Province, China; Sanming Project of Medicine in Shenzhen, China (grant number SZSM201911014); and donations from May Tam Mak Mei Yin, Richard Yu

and Carol Yu, the Shaw Foundation Hong Kong, Michael Seak-Kan Tong, Lee Wan Keung Charity Foundation Ltd, Hong Kong Sanatorium & Hospital, Hui Ming, Hui Hoy and Chow Sin Lan Charity Fund Ltd, Chan Yin Chuen Memorial Charitable Foundation, Marina Man-Wai Lee, the Hong Kong Hainan Commercial Association South China Microbiology Research Fund, the Jessie and George Ho Charitable Foundation, Perfect Shape Medical Ltd, Kai Chong Tong, Foo Oi Foundation Ltd, Tse Kam Ming Laurence, Betty Hing-Chu Lee, Ping Cham So, and Lo Ying Shek Chi Wai Foundation.

***Potential conflicts of interest.*** The authors: No reported conflicts of interest. All authors have submitted the ICMJE Form for Disclosure of Potential Conflicts of Interest.

## References

1. World Health Organization. Weekly epidemiological update—3 November 2020. Available at: https://www.who.int/docs/default-source/coronaviruse/situation-reports/weekly-epi-update-12.pdf?sfvrsn=c5d1b6fc_2&download=true. Accessed 11 June 2020.
2. Chan JF-W, Yuan S, Kok K-H, et al. A familial cluster of pneumonia associated with the 2019 novel coronavirus indicating person-to-person transmission: a study of a family cluster. Lancet **2020**; 395:514–23.
3. Hung IF, Cheng VC, Li X, et al. SARS-CoV-2 shedding and seroconversion among passengers quarantined after disembarking a cruise ship: a case series. Lancet Infect Dis **2020**; 20:1051–60.
4. Cheng VC, Wong SC, Chuang VW, et al. The role of community-wide wearing of face mask for control of coronavirus disease 2019 (COVID-19) epidemic due to SARS-CoV-2. J Infect **2020**; 81:107–14.
5. Li X, Sridhar S, Chan JF-W. The coronavirus disease 2019 pandemic: how does it spread and how do we stop it? Curr Opin HIV AIDS **2020**; 15:328–35.
6. Slifka MK, Gao L. Is presymptomatic spread a major contributor to COVID-19 transmission? Nat Med **2020**; 26:1531–3.
7. To KK, Tsang OT, Leung WS, et al. Temporal profiles of viral load in posterior oropharyngeal saliva samples and serum antibody responses during infection by SARS-CoV-2: an observational cohort study. Lancet Infect Dis **2020**; 20:565–74.
8. Peiris JS, Chu CM, Cheng VC, et al; HKU/UCH SARS Study Group. Clinical progression and viral load in a community outbreak of coronavirus-associated SARS pneumonia: a prospective study. Lancet **2003**; 361:1767–72.
9. To KK-W, Cheng VC-C, Cai J-P, et al. Seroprevalence of SARS-CoV-2 in Hong Kong and in residents evacuated from Hubei province, China: a multicohort study. Lancet Microbe **2020**; 1:E111–18.
10. World Health Organization. Coronavirus disease (COVID-19): similarities and differences with influenza. Available at: https://www.who.int/news-room/q-a-detail/coronavirus-disease-covid-19-similarities-and-differences-with-influenza. Accessed 11 June 2020.
11. Cheng VC, To KK, Tse H, Hung IF, Yuen KY. Two years after pandemic influenza A/2009/H1N1: what have we learned? Clin Microbiol Rev **2012**; 25:223–63.
12. Lansbury L, Lim B, Baskaran V, Lim WS. Co-infections in people with COVID-19: a systematic review and meta-analysis. J Infect **2020**; 81:266–75.
13. Stowe J, Tessier E, Zhao H, et al. Interactions between SARS-CoV-2 and Influenza and the impact of coinfection on disease severity: a test negative design. medRxiv [Preprint]. Posted online 22 September **2020**. doi:10.1101/2020.09.18.20189647.
14. Domenech de Celles M, Casalegno J-S, Lina B, Opatowski L. Influenza may facilitate the spread of SARS-CoV-2. medRxiv [Preprint]. 9 September **2020**. doi:10.1101/2020.09.07.20189779.
15. Liang L, He C, Lei M, et al. Pathology of guinea pigs experimentally infected with a novel reovirus and coronavirus isolated from SARS patients. DNA Cell Biol **2005**; 24:485–90.
16. Chan JF, Zhang AJ, Yuan S, et al. Simulation of the clinical and pathological manifestations of coronavirus disease 2019 (COVID-19) in golden Syrian hamster model: implications for disease pathogenesis and transmissibility [manuscript published online ahead of print 26 March 2020]. Clin Infect Dis **2020**. doi:10.1093/cid/ciaa325.
17. Chan JF-W, Yuan S, Zhang AJ, et al. Surgical mask partition reduces the risk of non-contact transmission in a golden Syrian hamster model for coronavirus disease 2019 (COVID-19) [manuscript published online ahead of print 30 May 2020]. Clin Infect Dis **2020**; 71(16):2139-49.
18. Iwatsuki-Horimoto K, Nakajima N, Ichiko Y, et al. Syrian hamster as an animal model for the study of human influenza virus infection. J Virol **2018**; 92:e01693-17.
19. Mok BW-Y, Cremin CJ, Lau S-Y, et al. SARS-CoV-2 spike D614G variant exhibits highly efficient replication and transmission in hamsters. bioRxiv [Preprint]. Posted online 28 August **2020**. doi:10.1101/2020.08.28.271635.
20. Zheng B, Chan KH, Zhang AJ, et al. D225G mutation in hemagglutinin of pandemic influenza H1N1 (2009) virus enhances virulence in mice. Exp Biol Med **2010**; 235:981–8.
21. Chan JF, Yip CC, To KK, et al. Improved molecular diagnosis of COVID-19 by the novel, highly sensitive and specific COVID-19-RdRp/Hel real-time reverse transcription-PCR assay validated in vitro and with clinical specimens. J Clin Microbiol **2020**; 58:e00310-20.
22. Lee ACY, To KKW, Zhu H, et al. Avian influenza virus A H7N9 infects multiple mononuclear cell types in peripheral blood and induces dysregulated cytokine responses and apoptosis in infected monocytes. J Gen Virol **2017**; 98: 922–34.
23. Chu H, Chan JF-W, Yuen TT-T, et al. Comparative tropism, replication kinetics, and cell damage profiling of SARS-CoV-2 and SARS-CoV with implications for clinical manifestations, transmissibility, and laboratory studies of COVID-19: an observational study. Lancet Microbe **2020**; 1:e14–23.
24. Zhang AJX, Zhu H, Chen Y, et al. Prostaglandin E2-mediated impairment of innate immune response to A(H1N1)pdm09 infection in diet-induced obese mice could be restored by paracetamol. J Infect Dis **2019**; 219:795–807.
25. Yuan S, Wang R, Chan JF, et al. Metallodrug ranitidine bismuth citrate suppresses SARS-CoV-2 replication and relieves virus-associated pneumonia in Syrian hamsters. Nat Microbiol **2020**; 5:1439–48.
26. Lee AC, Zhang AJ, Chan JF, et al. Oral SARS-CoV-2 inoculation establishes subclinical respiratory infection with virus shedding in golden Syrian hamsters. Cell Rep Med **2020**; 1:100121.
27. Zhang AJ, Lee AC-Y, Chu H, et al. Severe acute respiratory syndrome coronavirus 2 infects and damages the mature and immature olfactory sensory neurons of hamsters [manuscript published online ahead of print 15 July 2020]. Clin Infect Dis **2020**. doi:10.1093/cid/ciaa995.
28. Chu H, Chan JF, Wang Y, et al. Comparative replication and immune activation profiles of SARS-CoV-2 and SARS-CoV in human lungs: an ex vivo study with implications for the pathogenesis of COVID-19. Clin Infect Dis **2020**; 71:1400–9.
29. Zhang AJ, To KK, Li C, et al. Leptin mediates the pathogenesis of severe 2009 pandemic influenza A(H1N1) infection associated with cytokine dysregulation in mice with diet-induced obesity. J Infect Dis **2013**; 207:1270–80.
30. Lee AC, Zhu H, Zhang AJ, et al. Suboptimal humoral immune response against influenza A(H7N9) virus is related to its internal genes. Clin Vaccine Immunol **2015**; 22:1235–43.
31. Meskill SD, O'Bryant SC. Respiratory virus co-infection in acute respiratory infections in children. Curr Infect Dis Rep **2020**; 22:3.
32. Asner SA, Science ME, Tran D, Smieja M, Merglen A, Mertz D. Clinical disease severity of respiratory viral co-infection versus single viral infection: a systematic review and meta-analysis. PLoS One **2014**; 9:e99392.
33. Yue H, Zhang M, Xing L, et al. The epidemiology and clinical characteristics of co-infection of SARS-CoV-2 and influenza viruses in patients during COVID-19 outbreak [manuscript published online ahead of print 12 June 2020]. J Med Virol **2020**. doi:10.1002/jmv.26163.
34. Kumar N, Sharma S, Barua S, Tripathi BN, Rouse BT. Virological and immunological outcomes of coinfections. Clin Microbiol Rev **2018**; 31:e00111-17.
35. Gonzalez AJ, Ijezie EC, Balemba OB, Miura TA. Attenuation of influenza a virus disease severity by viral coinfection in a mouse model. J Virol **2018**; 92:e00881-18.
36. Chan KF, Carolan LA, Korenkov D, et al. Investigating viral interference between influenza a virus and human respiratory syncytial virus in a ferret model of infection. J Infect Dis **2018**; 218:406–17.
37. Muñoz-Fontela C, Dowling WE, Funnell SGP, et al. Animal models for COVID-19. Nature **2020**; 586:509–15.
38. Wang P, Zheng M, Lau SY, et al. Generation of DelNS1 Influenza Viruses: a Strategy for Optimizing Live Attenuated Influenza Vaccines. mBio **2019**; 10:e02180–19.